

Bi-level Dynamic Learning for Jointly Multi-modality Image Fusion and Beyond

Zhu Liu¹, Jinyuan Liu², Guanyao Wu¹, Long Ma¹, Xin Fan³ and Risheng Liu^{3*}

¹School of Software Technology, Dalian University of Technology, China

²School of Mechanical Engineering, Dalian University of Technology, China

³International School of Information Science Engineering, Dalian University of Technology, China

liuzhu@mail.dlut.edu.cn, atlantis918@hotmail.com, rsliu@dlut.edu.cn

Abstract

Recently, multi-modality scene perception tasks, e.g., image fusion and scene understanding, have attracted widespread attention for intelligent vision systems. However, early efforts always consider boosting a single task unilaterally and neglecting others, seldom investigating their underlying connections for joint promotion. To overcome these limitations, we establish the hierarchical dual tasks-driven deep model to bridge these tasks. Concretely, we firstly construct an image fusion module to fuse complementary characteristics and cascade dual task-related modules, including a discriminator for visual effects and a semantic network for feature measurement. We provide a bi-level perspective to formulate image fusion and follow-up downstream tasks. To incorporate distinct task-related responses for image fusion, we consider image fusion as a primary goal and dual modules as learnable constraints. Furthermore, we develop an efficient first-order approximation to compute corresponding gradients and present dynamic weighted aggregation to balance the gradients for fusion learning. Extensive experiments demonstrate the superiority of our method, which not only produces visually pleasant fused results but also realizes significant promotion for detection and segmentation than the state-of-the-art approaches.

1 Introduction

In real-world scenarios, multi-sensor vision systems play a fundamental role in intelligent applications, e.g., autonomous driving and robotics. With the rapid deployment of sensor hardware, how utilizing multi-modality images to provide comprehensive scene parsing become an urgent issue [Liu *et al.*, 2020; Jiang *et al.*, 2022; Liu *et al.*, 2021c]. Among them, infrared and visible sensors are two widely-used devices, aiming to capture the complete scene information. In detail, visible images can effectively describe the texture details but are sensitive to illumination changes. Infrared images can effectively highlight thermal targets but

lack texture details. Thus, combining the diverse modalities into one image to preserve complementary characteristics is a significant way for both observation [Xu *et al.*, 2022; Zhao *et al.*, 2023b] and understanding [Li *et al.*, 2022; Zhao *et al.*, 2022; Ma *et al.*, 2022].

Benefiting from the effective feature extraction of deep learning, various learning-based image fusion approaches have been developed, which can be divided into two mainstream categories, *i.e.*, auto-encoders [Liu *et al.*, 2021a; Li and Wu, 2018] and end-to-end learning approaches [Xu *et al.*, 2022; Zhang and Ma, 2021; Liu *et al.*, 2023]. As for auto-encoders, ℓ_1 norm [Li and Wu, 2018], weighted average [Liu *et al.*, 2021a] and maxing choose [Zhao *et al.*, 2020] are widely used for fuse features from pretrained auto-encoders. Introducing diverse statistic measurements (*e.g.*, modal gradients [Zhang and Ma, 2021] and image quality assessment [Xu *et al.*, 2022]), various end-to-end learning methods are proposed by designing effective architectures. However, we argue that most fusion methods focus on visual quality, ignoring the role to facilitate the downstream perception tasks. Constrained by the visual statistics, typical features, both benefit for visual quality and perception, are easy to be neglected, causing insufficient learning of both tasks.

Lately, few works [Liu *et al.*, 2022a; Tang *et al.*, 2022; Sun *et al.*, 2022] attempt to jointly realize the pixel-wise image fusion and semantic perception tasks. These works mostly cascade related networks directly and utilize end-to-end training with multi-task loss functions to realize task-driven image fusion. Unfortunately, there are two shortcomings that limit their performance. (i) *Lacking the investigation of underlying connection*: Joint learning may place an obstacle to preserving distinct features of tasks and cannot formulate intrinsic mutual-promoted relationships. (ii) *Inflexible trade-off of multi-task learning*: Existing methods mostly utilize manual hyper-parameters to balance the diverse loss functions, which cannot guarantee optimal performances for both tasks. Thus, the primary goal of this paper is to realize comprehensive image fusion, in order to achieve joint promotion both for observation and semantic understanding.

1.1 Our Contribution

To mitigate these issues, we develop a generic bi-level dynamic learning paradigm for bridging the relationships jointly between multi-modality image fusion and semantic percep-

*Corresponding author

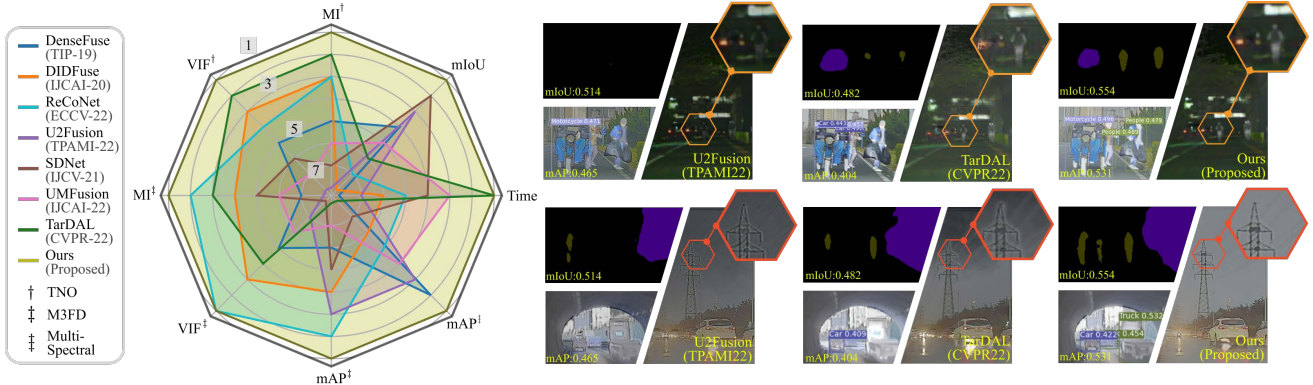


Figure 1: Comprehensive comparisons with advanced multi-modality image fusion methods on visual quality, object detection, and segmentation. The left figure plots the rankings on diverse metrics with four datasets. The right figures depict the visual comparisons.

tion tasks. Concretely, we first establish a hierarchical deep model, composited by an image fusion module, visual discriminator, and commonly used perception network. We introduce dual learnable modules for the measurement of visual quality and semantic perception respectively, to provide distinct task-specific responses for image fusion. More importantly, a bi-level learning paradigm is proposed to formulate the latent connection of hierarchical modules. We also derive a dynamic weighting aggregation with efficient approximation to realize the mutually reinforcing of visual results and perception jointly. Figure 1 demonstrates our proposed strategy achieves better visual-appealing fused images and precise semantic perception performance (detection and segmentation) against state-of-the-arts. Our contributions can be concluded as follows:

- Considering the visual quality and semantic information richness of image fusion as two correlative goals, we propose a hierarchical deep model to realize the mutually reinforced task-driven image fusion.
- For the training strategy, we devise a bi-level formulation to bridge the image fusion with two task-specific constraints, providing an efficient way to formulate their inner mutual-benefit relationship.
- For the solving procedure, we drive a dynamic aggregated solution, yielding the efficient gradient approximation and adaptive weighting schemes to balance the gradients from diverse modules automatically, for learning the optimal parameters for both tasks.
- Comprehensive evaluations on three multi-modality vision tasks (*i.e.*, image fusion, object detection, and semantic segmentation) are conducted to illustrate the superiority against state-of-the-art methods. Sufficient analytical results also substantiate the effectiveness.

2 The Proposed Method

2.1 Motivation

As aforementioned, the most straightforward way is to establish cascaded architectures [Liu *et al.*, 2022a; Tang *et al.*, 2022; Zhao *et al.*, 2023a] (denoted as \mathcal{N}) for realizing the

Algorithm 1 Dynamic Aggregated Solution.

Require: Multi-modality inputs \mathbf{x}, \mathbf{y} , loss function ϕ_V, ϕ_P , and Φ and other necessary hyper-parameters.

- 1: Preparing pairs $\{\mathbf{x}, \mathbf{y}\}$ with perception labels \mathbf{z}^* .
- 2: % Warm start phase.
- 3: Pretrain the fusion network \mathcal{F} for initializing ω .
- 4: **while** not converged **do**
- 5: $\theta_V \leftarrow \theta_V - \nabla_{\theta_V} \phi_V(\mathcal{T}_V(\mathbf{u}; \theta_V(\omega)))$.
- 6: $\theta_P \leftarrow \theta_P - \nabla_{\theta_P} \phi_P(\mathcal{T}_P(\mathbf{u}; \theta_P(\omega)))$.
- 7: Calculate gradient \mathbf{G}_V and \mathbf{G}_P with Eq. (4).
- 8: Generate λ_V and λ_P by using RLW.
- 9: $\omega \leftarrow \omega - (\lambda_V \mathbf{G}_V + \lambda_P \mathbf{G}_P)$.
- 10: **end while**
- 11: **return** ω^*, θ_P^* .

comprehensive perception. These networks can be directly decomposed as an image fusion module (denoted as \mathcal{F}) and a task-oriented module (denoted as \mathcal{T}). These mainstream architectures can be formulated as $\mathcal{N} = \mathcal{F} \circ \mathcal{T}$, training by the combination of diverse loss functions. We argue that existing methods rely on handcrafted visual measurements, which are not adaptative and flexible for joint learning. Thus, we propose a hierarchical dual-tasks driven model. In detail, as for image fusion, we introduce two dense residual blocks [Yan *et al.*, 2019] to composite the network \mathcal{F} with parameters ω , to maintain the complementary characteristics from source images for generating fused images \mathbf{u} . Supposing infrared and visible images as \mathbf{x} and \mathbf{y} with gray-scale, the fusion learning can be written as $\mathbf{u} = \mathcal{F}(\mathbf{x}, \mathbf{y}; \omega)$. In order to measure the adaptive intensity distribution, we introduce a discriminator as \mathcal{T}_V with parameters θ_V to measure the texture similarity with source images. Denoted the classified output as \mathbf{z}_V , the discrimination can be formulated as $\mathbf{z}_V = \mathcal{T}_V(\mathbf{u}; \theta_V)$. This formulation can provide adaptive learnable responses, compared with handcrafted loss functions.

Moreover, as for the semantic understanding, two representative networks for object detection [Tian *et al.*, 2019] and semantic segmentation [Xie *et al.*, 2021] are selected as the task module \mathcal{T}_P with parameters θ_P . Similarly, the task solution can be written as $\mathbf{z}_P = \mathcal{T}_P(\mathbf{u}; \theta_P)$. Thus, the complete

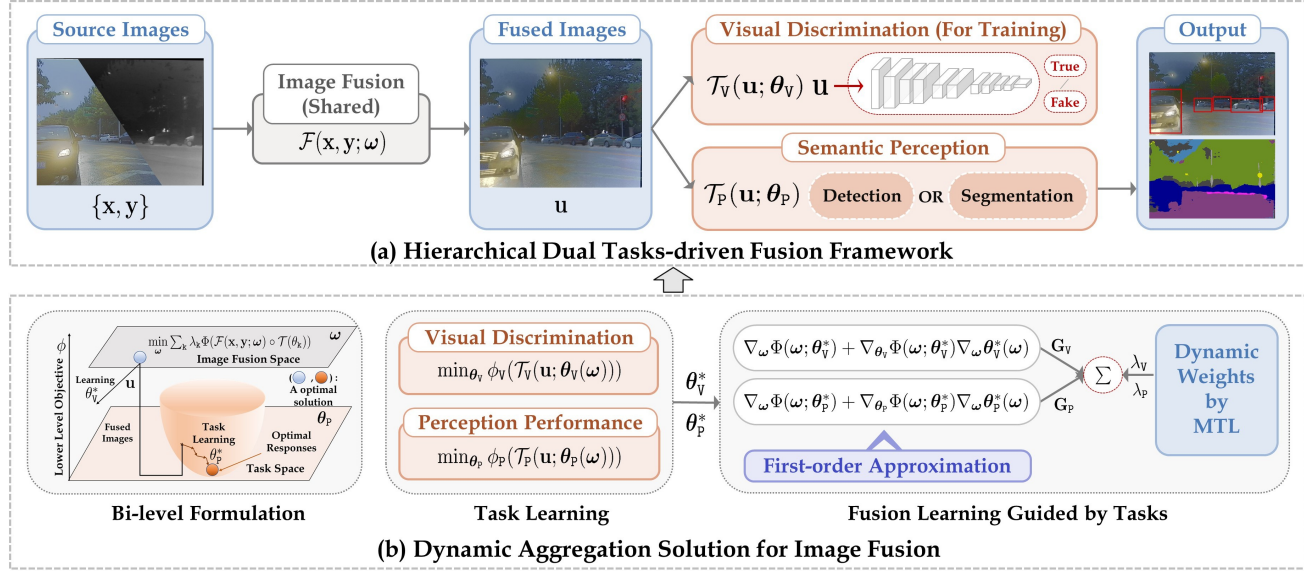


Figure 2: Schematic of the proposed model and strategy. In (a), we plot the hierarchical dual-tasks driven fusion framework on the training and inference phase respectively. The proposed bi-level formulation with a concrete learning procedure is shown at (b).

cascaded architecture can be formulated as:

$$\begin{cases} \mathbf{u} = \mathcal{F}(\mathbf{x}, \mathbf{y}; \omega), \\ \mathbf{z}_k = \mathcal{T}_k(\mathbf{u}; \theta_k), \end{cases} \quad (1)$$

where $k \in \{V, P\}$ and the workflow is shown in Figure 2 (a). Specifically, compared with multi-task learning, the fusion network \mathcal{F} actually plays a role for robust feature extraction (can be viewed as “encoder”). \mathcal{T}_V and \mathcal{T}_P are as task-specific “decoders” introduced to learn the ability to discriminate fusion quality and measure the informative richness to support the downstream scene perception.

2.2 Bi-level Formulation

Recently, various training strategies are proposed to address the high-level task-driven image fusion, including unrolled end-to-end training [Liu *et al.*, 2022a], separate stage-wise training [Wu *et al.*, 2022] and adaptive loop-based training [Tang *et al.*, 2022]. However, we emphasize that these optimization strategies cannot model the coupled mutual-benefit relationship between visual quality and semantic reinterpretation, which is untoward to balance the influences of distinct tasks. Therefore, designing the learning paradigm to realize the “Best of Both Worlds” simultaneously is the core goal of this paper. In this part, we provide a bi-level formulation to depict the overall optimization procedure, in order to illustrate the mutual collaboration and guidance between visual inspection and semantic perception. The bi-level learning [Liu *et al.*, 2021b] can be formulated as:

$$\min_{\omega} \sum_k \lambda_k \Phi_k(\mathcal{F}(\mathbf{x}, \mathbf{y}; \omega) \circ \mathcal{T}_k(\theta_k)), \quad (2)$$

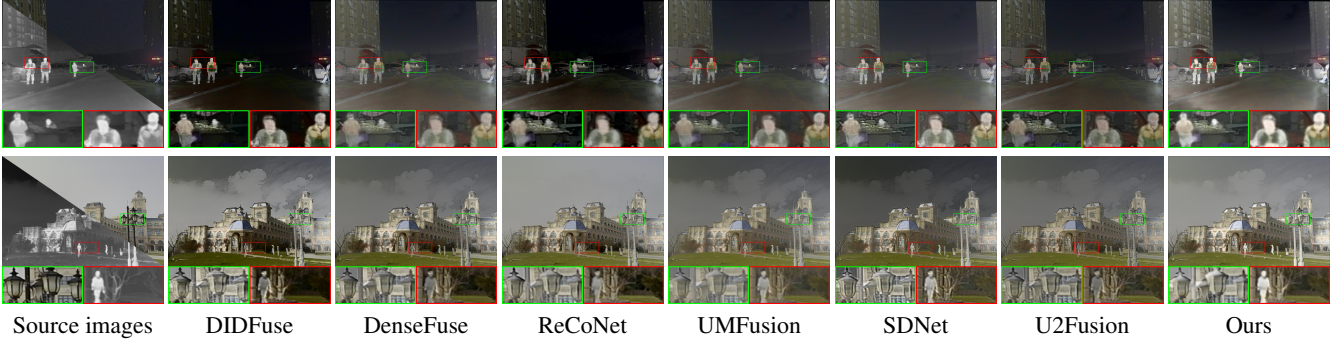
$$\text{s.t. } \begin{cases} \theta_V^* = \arg \min_{\theta_V} \phi_V(\mathcal{T}_V(\mathbf{u}; \theta_V(\omega))), \\ \theta_P^* = \arg \min_{\theta_P} \phi_P(\mathcal{T}_P(\mathbf{u}; \theta_P(\omega))), \end{cases} \quad (3)$$

where $\mathbf{u} = \mathcal{F}(\mathbf{x}, \mathbf{y}; \omega^*)$. Φ and ϕ are the objectives on the validation and training datasets respectively. λ_k represents the dynamic multi-task trade-off parameters. To be more specific, the primary part is to optimize the fusion network \mathcal{F} for extracting rich features, which can be a benefit for the visual quality and semantic perception, expressed by Eq. (2). Furthermore, the discrimination of visual effects and responses of semantic understanding are two vital constraints to provide diverse task-specific information, as shown in Eq. (3). On the other hand, the hierarchical formulation between Eq. (2) and Eq. (3) are nested with mutual promotion. Fused images \mathbf{u} are the fundamental data dependency for following task learning. Based on the responses from vision tasks, task-driven feedback can assist in the optimization of fusion from downstream vision tasks.

2.3 Dynamic Aggregation Solution

This part details the solution to address the aforementioned bi-level formulation (Eq. (2) and Eq. (3)). In order to accelerate the training convergence, we first introduce a warm-start strategy to pretrain the fusion network. Then, we present a dynamic aggregation solution to jointly address fusion and perception. The concrete optimization procedure is shown in Figure 2 (b). It actually can be expressed with hierarchical optimization, *i.e.*, task learning (Eq. (3)) and task-guided fusion learning (Eq. (2)). Following with existing practical strategies [Liu *et al.*, 2021b], we first optimize the lower-level task constraints with several steps to estimate the optimal parameters θ_V^* and θ_P^* , in order to learn the measurement for visual quality and perception based on task-specific losses.

Considering the mutual influence between fusion and lower vision tasks, represented by $\theta_k(\omega)$, $k \in \{V, P\}$, there actually exists a complicated connection between the hierarchical tasks, which can be used to measure the response of tasks facing with the changes of fused images. As for the op-

Figure 3: Visual comparison of different fusion approaches on two challenging scenarios (*i.e.*, extreme darkness and small targets).

Datasets	Metrics	DDcGAN	DenseFuse	AUIF	DIDFuse	MFEIF	ReCoNet	UMIFusion	SDNet	U2Fusion	TarDAL	Ours
TNO	MI↑	1.737	2.248	2.181	2.349	2.496	2.349	2.071	1.952	1.811	2.648	2.946
	VIF↑	0.683	0.798	0.819	0.832	0.783	0.824	0.695	0.754	0.678	0.860	0.913
	FMI↑	0.858	0.890	0.879	0.863	0.891	0.878	0.888	0.883	0.879	0.881	0.892
RoadScene	MI↑	2.569	3.044	3.066	3.103	3.225	3.099	2.748	3.113	3.328	3.391	3.526
	VIF↑	0.577	0.755	0.842	0.793	0.767	0.750	0.742	0.768	0.698	0.745	0.897
	FMI↑	0.859	0.868	0.856	0.853	0.870	0.858	0.866	0.863	0.861	0.852	0.871
M3FD	MI↑	2.148	2.384	2.399	2.520	2.689	2.754	2.470	2.512	2.178	2.558	3.033
	VIF↑	0.570	0.600	0.682	0.685	0.645	0.699	0.585	0.533	0.563	0.661	0.699
	FMI↑	0.836	0.863	0.845	0.831	0.848	0.845	0.855	0.846	0.850	0.825	0.863

Table 1: Quantitative results of visual fusion quality on three representative datasets with ten competitive methods.

timization of image fusion, dual gradients can be obtained, which can be written as:

$$\begin{cases} \mathbf{G}_V = \nabla_{\omega} \Phi_V(\omega; \theta_V^*) + \nabla_{\theta_V} \Phi_V(\omega; \theta_V^*) \nabla_{\omega} \theta_V^*(\omega), \\ \mathbf{G}_P = \nabla_{\omega} \Phi_P(\omega; \theta_P^*) + \nabla_{\theta_P} \Phi_P(\omega; \theta_P^*) \nabla_{\omega} \theta_V^*(\omega), \end{cases} \quad (4)$$

In detail, the gradient \mathbf{G}_V and \mathbf{G}_P are computed by $\Phi_k(\mathcal{F}(\mathbf{x}, \mathbf{y}; \omega) \circ \mathcal{T}_k(\theta_k))$. The first term is a direct gradient in term of ω and the second term depicts the latent coupled connection with follow-up perception tasks.

First-order approximation. In literature, solving Eq. (4) is a challenging issue, where the bottleneck is to compute the second-order gradient (the second term). Inspired by the Gaussian-Newton approximation, which provides a first-order computation to address continuous learning [Zhou *et al.*, 2021a] and generative adversarial learning [Liu *et al.*, 2022b], we introduce this strategy to approximate the Hessian in gradients \mathbf{G}_V and \mathbf{G}_P . Based on the implicit function theory, we can drive that $\nabla_{\omega} \theta(\omega) = -\nabla_{\omega, \theta}^2 \Phi(\omega; \theta) \nabla_{\theta, \theta}^2 \Phi(\omega; \theta)^{-1}$. Gaussian-Newton approximation can convert the complicated Hessian matrix with the production of first-order vectors, *i.e.*,

$$\nabla_{\omega} \theta(\omega) \approx \frac{\nabla_{\theta} \Phi(\omega; \theta)^T \nabla_{\theta} \phi(\omega; \theta)}{\nabla_{\theta} \phi(\omega; \theta)^T \nabla_{\theta} \phi(\omega; \theta)} \nabla_{\omega} \phi(\omega; \theta). \quad (5)$$

Dynamic gradient aggregation. Another challenging issue is how to adaptively balance the gradients \mathbf{G}_V and \mathbf{G}_P to jointly optimize the image fusion network \mathcal{F} . Recently, Random Loss Weighting (RLW) [Lin *et al.*, 2022] is advanced in

Multi-Task Learning (MTL), which can avoid the local minima with higher generalization and comparable performance. We leverage normal distribution $p(\lambda)$ to generate λ_V and λ_P , to avoid the focus on one strongly correlated task and ignoring another. The whole solution is summarized in Alg. 1.

2.4 Loss Functions

In this part, we will elaborate the concrete loss functions to define ϕ and Φ respectively, which can be divided into two parts for visual quality and semantic perception respectively.

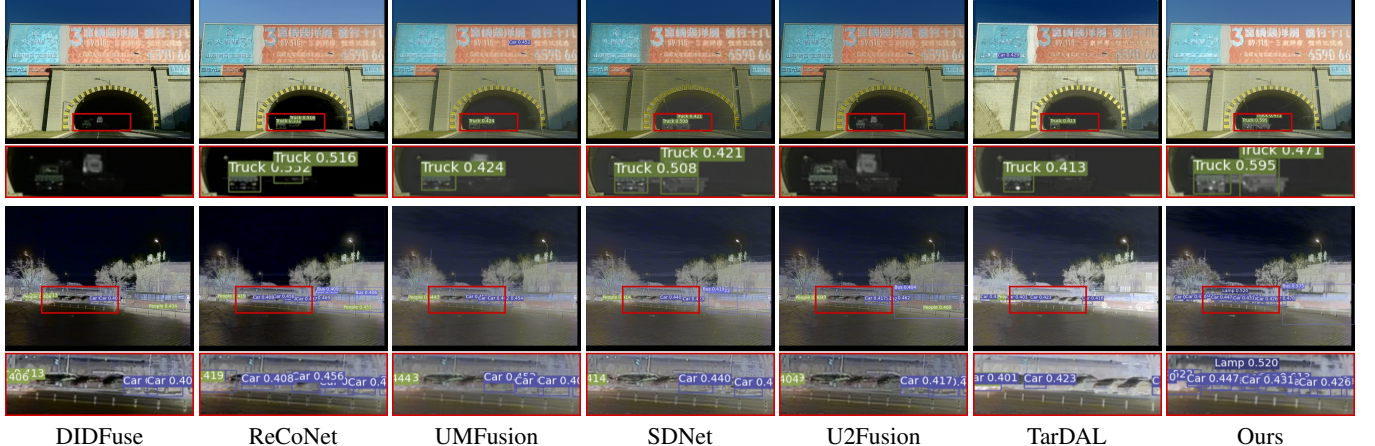
As for the learning of discriminator \mathcal{T}_V [Isola *et al.*, 2017], we introduce the generative adversarial mechanism to discriminate the visual quality of image fusion. In concrete, we first construct the pseudo fused images \mathbf{u}_m to maintain the salient informations by saliency weight maps (\mathbf{m}_1 and \mathbf{m}_2) using VSM [Ma *et al.*, 2017], *i.e.*, $\mathbf{u}_m = \mathbf{m}_1 \mathbf{x} + \mathbf{m}_2 \mathbf{y}$. We also gradient-penalty Wasserstein strategy [Gulrajani *et al.*, 2017] to guarantee the learning stability, thus the concrete formulation to train \mathcal{T}_V can be written as

$$\phi_V = \mathbb{E}_{\tilde{\mathbf{s}} \sim \mathbb{P}_{\text{fake}}} \mathcal{T}_V(\mathbf{u}) - \mathbb{E}_{\mathbf{s} \sim \mathbb{P}_{\text{real}}} \mathcal{T}_V(\mathbf{u}_m) + \eta R_{\text{Penalty}}, \quad (6)$$

where R_{Penalty} is the penalty term, calculated by $\mathbb{E}_{\tilde{\mathbf{s}} \sim \mathbb{P}_{\text{fake}}} [(\|\nabla_{\mathbf{u}} \mathcal{T}_V(\mathbf{u})\|_2 - 1)^2]$ and η is a trade-off term.

Furthermore, image fusion network \mathcal{F} can be considered as the generator. In order to balance the pixel intensity and avoid the texture artifact, we also leverage the pixel error loss for the fusion learning, *i.e.*,

$$\Phi_V = \|\mathbf{u} - \mathbf{m}_1 \mathbf{x}\|_2^2 + \|\mathbf{u} - \mathbf{m}_2 \mathbf{y}\|_2^2 - \mathbb{E}_{\mathbf{s} \sim \mathbb{P}_{\text{real}}} \mathcal{T}_V(\mathbf{u}). \quad (7)$$

Figure 4: Detection comparison with advanced approaches under two difficult scenarios (*i.e.*, tunnel and dense objects in the darkness).

Methods	M3FD						Multi-Spectral						Efficiency Analysis			
	Lamp	Car	Bus	Motor	Truck	People	mAP↑	CStop	Car	Person	Bump	Bike	mAP↑	Size(M)↓	FLOPs(G)↓	Time(S)↓
DDcGAN	0.247	0.664	0.451	0.312	0.355	0.444	0.412	0.312	0.360	0.199	0.167	0.347	0.277	1.097	896.84	0.211
DenseFuse	0.249	0.694	0.432	0.319	0.346	0.501	0.424	0.425	0.515	0.541	0.377	0.409	0.453	0.074	48.96	0.251
AUIF	0.244	0.693	0.406	0.282	0.326	0.496	0.408	0.387	0.528	0.479	0.222	0.424	0.408	0.012	0.014	0.166
DIDFuse	0.300	0.722	0.373	0.305	0.444	0.536	0.466	0.368	0.490	0.504	0.277	0.373	0.402	0.373	103.56	0.118
MEEIF	0.285	0.719	0.442	0.321	0.418	0.540	0.454	0.432	0.531	0.539	0.377	0.419	0.460	0.705	48.92	0.141
ReCoNet	0.336	0.744	0.482	0.311	0.445	0.556	0.479	0.401	0.507	0.401	0.377	0.397	0.417	0.209	12.54	0.051
UMFusion	0.254	0.692	0.424	0.309	0.343	0.518	0.423	0.389	0.525	0.504	0.361	0.439	0.442	0.629	174.69	0.044
SDNet	0.265	0.702	0.429	0.344	0.331	0.515	0.431	0.359	0.503	0.495	0.167	0.433	0.391	0.067	37.35	0.045
U2Fusion	0.312	0.724	0.475	0.352	0.392	0.534	0.465	0.419	0.542	0.501	0.333	0.453	0.449	0.659	366.34	0.123
TarDAL	0.229	0.652	0.425	0.285	0.317	0.515	0.404	0.343	0.495	0.513	0.167	0.392	0.382	0.297	82.37	0.001
Ours	0.351	0.759	0.511	0.413	0.551	0.598	0.531	0.423	0.586	0.574	0.479	0.525	0.504	0.417	106.02	0.001

Table 2: Quantitative results of object detection on the M3FD and Multi-Spectral datasets and efficiency analysis. The best result is in red whereas the second best one is in blue.

As for the semantic perception optimization of \mathcal{T}_P , we adopt the common task-specific loss functions to training the perception-related objectives (*i.e.*, Φ_P and ϕ_P). For object detection, we utilize the hybrid loss functions from FCOS [Tian *et al.*, 2019] to define the objective. As for the semantic segmentation, common to previous literature, we utilize the cross-entropy loss function.

3 Experiments

3.1 Implementation Details

We implemented the experiments on five representative datasets (TNO, RoadScene [Xu *et al.*, 2022] and M3FD for visual evaluations, M3FD [Liu *et al.*, 2022a] and Multi-Spectral [Takumi *et al.*, 2017] for detection, and MFNet [Ha *et al.*, 2017] for segmentation). SGD optimizer is utilized to update the parameters of each module. As for the perception task, the initialized learning rate is $2e^{-4}$ and will be decreased to $2e^{-6}$ with a multi-step decay strategy. As for the optimization of fusion, we utilize the same learning rate. All experiments are implemented with the PyTorch framework and on an NVIDIA Tesla V100 GPU.

3.2 Evaluation in Multi-modality Image Fusion

We conducted qualitative and quantitative analyses with ten state-of-the-art competitors, including DDcGAN [Xu *et al.*, 2019], AUIF [Zhao *et al.*, 2021], MFEIF [Liu *et al.*, 2021a], SDNet [Zhang and Ma, 2021], DIDFuse [Zhao *et al.*, 2020], DenseFuse [Li and Wu, 2018], ReCoNet [Huang *et al.*, 2022], UMFusion [Wang *et al.*, 2022], TarDAL [Liu *et al.*, 2022a] and U2Fusion [Xu *et al.*, 2022].¹

Qualitative comparisons. The qualitative results on diverse challenging scenarios are depicted in Figure 3. It can be clearly observed that our method outperforms other methods in two eye-catching aspects. First, our method sufficiently reserves the high-contrast information from infrared images. For instance, in all scenarios, the buildings and pedestrians are best highlighted. Furthermore, our method reserves visible structure on the premise of retaining significant infrared characteristics. Overall, our method highlights the vital information (*e.g.*, pedestrians) and suppresses the disturbing information (*e.g.*, large darkness).

¹“Fusion with detection” is selected for comparison.

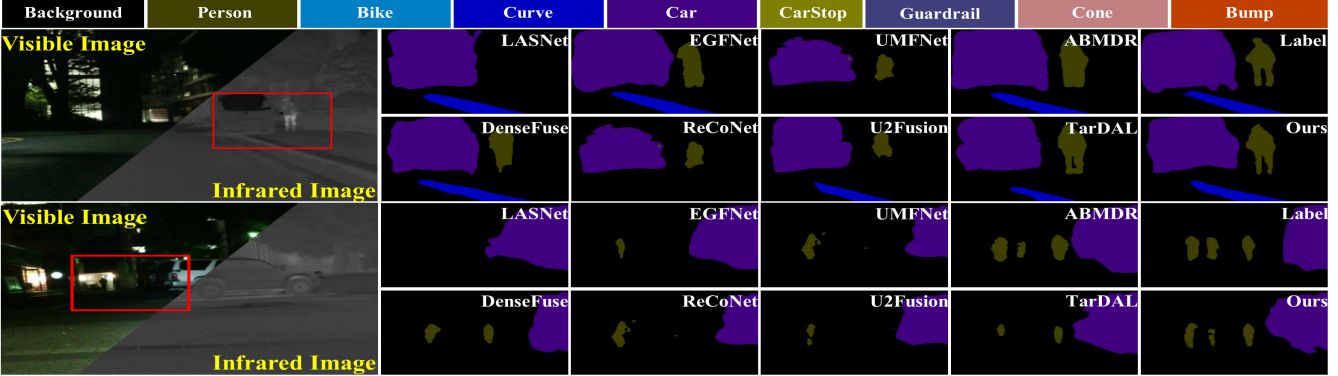


Figure 5: Qualitative comparisons with eight advanced competitors under nighttime on the MFNet benchmark.

Methods	Unlabel		Car		Person		Bike		Curve		Car Stop		Cone		Bump		mAcc↑	mIoU↑
	Acc↑	IoU↑	Acc↑	IoU↑	Acc↑	IoU↑	Acc↑	IoU↑	Acc↑	IoU↑	Acc↑	IoU↑	Acc↑	IoU↑	Acc↑	IoU↑	Acc↑	IoU↑
LASNet	99.2	97.4	94.9	84.2	81.7	67.1	82.1	56.9	70.7	41.1	56.8	39.6	58.1	48.8	77.2	40.1	75.4	54.9
EGFNet	99.3	97.7	95.7	87.6	89.0	69.8	80.6	58.8	71.5	42.8	48.7	33.8	65.3	48.3	71.1	47.1	72.7	54.8
ABMDR	99.3	98.4	94.3	84.8	90.0	69.6	75.7	60.3	64.0	45.1	44.1	33.1	61.7	47.4	66.2	50.0	69.5	54.8
DenseFuse	98.4	97.8	93.5	82.8	86.0	67.7	81.6	60.2	66.5	42.5	61.4	12.6	80.5	39.1	67.6	44.1	71.1	50.1
AUIF	97.9	97.4	95.1	80.2	80.8	54.0	78.4	57.0	68.8	27.0	62.2	30.1	81.9	40.0	96.5	24.8	73.8	45.8
DIDFuse	98.1	96.9	89.1	78.0	82.9	59.6	70.5	53.4	34.2	20.6	49.0	25.1	82.4	34.7	59.5	20.0	63.1	43.3
ReCoNet	97.9	97.2	96.0	79.3	85.4	60.9	77.5	58.2	43.2	22.6	56.8	32.8	73.5	36.7	36.2	13.5	63.0	44.6
UMFusion	98.1	97.5	95.4	81.4	88.7	62.5	78.5	60.1	47.8	25.5	61.2	26.2	67.6	39.6	85.6	46.8	69.6	49.1
SDNet	98.4	97.7	96.1	83.1	85.9	70.5	75.6	60.2	60.9	35.6	76.6	28.1	88.6	46.1	71.1	45.5	73.7	52.8
U2Fusion	98.3	97.7	94.3	82.7	87.0	64.1	78.9	61.0	56.2	35.5	75.2	24.0	80.5	46.3	81.3	49.9	72.6	51.4
TarDAL	98.4	97.5	89.2	79.5	87.1	67.3	77.0	59.9	53.3	29.1	72.5	22.0	84.2	35.6	70.6	40.4	70.6	48.2
SeaFusion	98.2	97.7	94.4	82.2	88.1	67.7	83.9	59.7	65.7	37.3	72.4	16.8	87.3	41.3	85.7	27.2	75.5	48.1
Ours	98.7	98.0	95.7	86.2	84.4	71.6	84.4	63.6	60.4	40.7	69.1	37.3	87.3	49.9	83.0	51.2	73.6	55.4

Table 3: Quantitative results of semantic segmentation with different methods on the MFNet dataset.

Quantitative comparisons. We also report the numerical results with the other ten fusion competitors on TNO, Road-Scene, and M3FD in Table 1. We adopt three objective metrics for analysis. We can clearly observe that our method demonstrates superiority in terms of these statistical metrics. Specifically, the highest MI and FMI indicate our method can effectively integrate source information, *e.g.*, edges and contrast. Moreover, the significant improvement of VIF implies that our method is consistent with human vision.

3.3 Comparing with SOTA in Object Detection

Qualitative comparisons. We visualize the object detection results in Figure 4. At the first row, it can be clearly observed that DIDFuse, TarDAL, and UMFusion lead to the classification or dislocation of the bounding box (*e.g.*, the truck to be detected completely). On the contrary, our method sufficiently preserves the information of categories and results in accurate detection. As for the detection of small targets, *i.e.*, in the second row, our method detects almost all cars while other methods lead to the omission.

Quantitative comparisons. The quantitative detection results are presented in Table 2. We can see that our method substantially outperforms other methods in terms of most

categories and realizes 10.8% and 9.6% higher detection mAP on the M3FD and Multi-Spectral datasets, respectively. Apart from detection results, we further conduct the efficiency analysis in Table 2. Obviously, benefiting from the dilated convolutions, the minimal time consumption indicates that our method achieves real-time image fusion.

3.4 Extension to Multi-modality Segmentation

Besides comparing with the advanced image fusion, we also provide the evaluations with three specifically-designed methods: EGFNet [Zhou *et al.*, 2021b], ABMDRNet [Zhang *et al.*, 2021] and LASNet [Li *et al.*, 2022].

Qualitative comparisons. We select two challenging scenarios to illustrate the remarkable performance compared with eight methods in Figure 5. Two significant advantages can be concluded from these instances. Firstly, our scheme can effectively preserve the complete structure of thermal-sensitive targets (*e.g.*, pedestrian) with precise prediction. For example, the pedestrian in the distance cannot be accurately estimated by most methods. Secondly, our scheme also highlights abundant texture details for the normal categories (*e.g.*, car and curve). Obviously, our method can precisely estimate the structure of cars on both image pairs.

Strategy	Fusion			Detection		
	MI↑	VIF↑	FMI↑	Car	Person	mAP↑
[Liu <i>et al.</i> , 2022a]	2.192	0.733	0.889	0.736	0.589	0.466
[Tang <i>et al.</i> , 2022]	2.210	0.751	0.891	0.660	0.509	0.384
Proposed	2.946	0.913	0.892	0.759	0.598	0.531

Table 4: Analyzing the proposed training strategy.

Quantitative comparisons. Table 3 reports the concrete numerical results on eight categories of the MFNet dataset. Specifically, compared with SeaFusion, which is a segmentation-driven method, our scheme drastically improves 15.2 % of mIOU. Noting that, only utilizing one backbone network, our method can achieve comparable performance with specially designed segmentation methods (e.g., LASNet and EGFNet). Especially, we achieve better accuracy in the classification of persons and cars, which is vital for the employment of intelligent vision systems.

Task	Metric	Manual	EW	GNorm	DWA	Ours
Fusion	MI↑	2.074	2.117	1.696	1.971	2.251
	VIF↑	0.741	0.756	0.347	0.728	0.772
	FMI↑	0.876	0.877	0.869	0.879	0.879
Detection	Car	0.673	0.670	0.683	0.651	0.711
	Person	0.471	0.498	0.474	0.509	0.536
	mAP↑	0.352	0.363	0.373	0.362	0.428

Table 5: Analyzing the aggregation strategy with finite epochs.

Model	Fusion			Detection		
	MI↑	VIF↑	FMI↑	Car	Person	mAP↑
TarDAL _J	2.558	0.661	0.825	0.652	0.515	0.404
TarDAL _P	2.465	0.614	0.843	0.714	0.555	0.440
UMFusion _J	2.470	0.585	0.855	0.692	0.518	0.408
UMFusion _P	2.999	0.653	0.881	0.712	0.523	0.452

Table 6: Evaluating of generalization ability on M3FD benchmark.

3.5 Ablation Studies

Effects of proposed training strategy. To demonstrate the effectiveness of the bi-level learning paradigm, we conduct the comparison with two mainstream training strategies (*i.e.*, unrolled training [Liu *et al.*, 2022a] and adaptive loop training [Tang *et al.*, 2022]). Table 4 reports the numerical results of image fusion and detection based on these strategies. Both existing strategies are concrete on one task and neglect another. We can observe that the proposed strategy achieves consistent performance for the two scene parsing tasks.

Evaluating of dynamic aggregation strategy. In order to evaluate the effectiveness of dynamic weights, we provide other four classical adjustment ways, *i.e.*, manual-design, equal weighting, gradient normalization [Chen *et al.*, 2018] and DWA [Liu *et al.*, 2019]. The numerical results (trained with 10 epochs) are reported in Table 5. The random aggregation can effectively avoid the local optimum with higher performance compared with representative multi-task learning and manual adjustment.

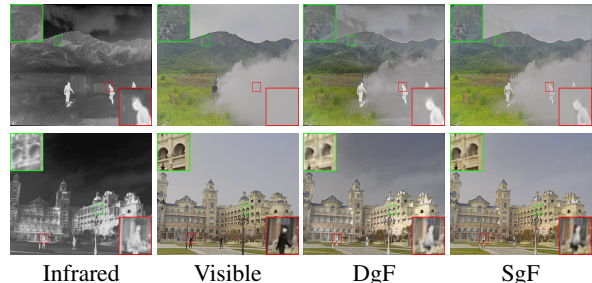


Figure 6: Visual differences of fusion guided by perception tasks.

Guided Task	TNO			M3FD		
	MI↑	VIF↑	FMI↑	MI↑	VIF↑	FMI↑
Detection	2.946	0.913	0.892	3.033	0.699	0.863
Segmentation	2.902	0.745	0.889	3.482	0.781	0.864

Table 7: Visual influences of perception tasks.

Evaluating of generalization ability. The proposed bi-level dynamic learning is a generalized scheme, which is network-agnostic. Table 6 illustrates the significant improvement for advanced fusion networks (*i.e.*, TarDAL and UMFusion) using our training strategy. Subscripts “J” and “P” denote the joint and proposed training strategies.

Influences of perception tasks for image fusion. We also analyze the influence of diverse perception guidance for image fusion in Table 7 and Figure 6 respectively. We can observe that both quantitative results are higher than current advanced methods. Detection-guided fusion (denoted as “DgF”) realizes better results on TNO, which contain abundant targets with high contrast. Segmentation-guided fusion (denoted as “SgF”) achieves a significant improvement on M3FD, which is with vivid texture details. From Figure 6, we can observe DgF tends to preserve the salient targets (*e.g.*, person). The results of SgF prefer to maintain the scene background with obvious structural information for pixel-wise classification.

4 Conclusion

In this paper, a hierarchical dual-task deep model was proposed to bridge multi-modality image fusion and semantic perception jointly. We presented a bi-level formulation to depict the coupled relationship, to realize mutual promotion. Then a dynamic aggregation strategy was proposed to combine the gradients from distinct tasks to achieve the comprehensive image fusion. Extensive experiments demonstrated our method is superior to address diverse vision tasks.

Acknowledgments

This work is partially supported by the National Key R&D Program of China (2020YFB1313503), the National Natural Science Foundation of China (U22B2052), the Fundamental Research Funds for the Central Universities and the Major Key Project of PCL (PCL2021A12).

References

- [Chen *et al.*, 2018] Zhao Chen, Vijay Badrinarayanan, Chen-Yu Lee, and Andrew Rabinovich. Gradnorm: Gradient normalization for adaptive loss balancing in deep multitask networks. In *ICML*, pages 794–803. PMLR, 2018.
- [Gulrajani *et al.*, 2017] Ishaan Gulrajani, Faruk Ahmed, Martin Arjovsky, Vincent Dumoulin, and Aaron C Courville. Improved training of wasserstein gans. *NeurIPS*, 30, 2017.
- [Ha *et al.*, 2017] Qishen Ha, Kohei Watanabe, Takumi Karasawa, Yoshitaka Ushiku, and Tatsuya Harada. Mfnet: Towards real-time semantic segmentation for autonomous vehicles with multi-spectral scenes. In *IROS*, pages 5108–5115. IEEE, 2017.
- [Huang *et al.*, 2022] Zhanbo Huang, Jinyuan Liu, Xin Fan, Risheng Liu, Wei Zhong, and Zhongxuan Luo. Reconet: Recurrent correction network for fast and efficient multi-modality image fusion. In *ECCV*, pages 539–555. Springer, 2022.
- [Isola *et al.*, 2017] Phillip Isola, Jun-Yan Zhu, Tinghui Zhou, and Alexei A Efros. Image-to-image translation with conditional adversarial networks. In *CVPR*, pages 1125–1134, 2017.
- [Jiang *et al.*, 2022] Zhiying Jiang, Zengxi Zhang, Xin Fan, and Risheng Liu. Towards all weather and unobstructed multi-spectral image stitching: Algorithm and benchmark. In *ACM MM*, pages 3783–3791, 2022.
- [Li and Wu, 2018] Hui Li and Xiao-Jun Wu. Densefuse: A fusion approach to infrared and visible images. *IEEE TIP*, 28(5):2614–2623, 2018.
- [Li *et al.*, 2022] Gongyang Li, Yike Wang, Zhi Liu, Xinpeng Zhang, and Dan Zeng. Rgb-t semantic segmentation with location, activation, and sharpening. *IEEE TCSVT*, 2022.
- [Lin *et al.*, 2022] Baijiong Lin, YE Feiyang, Yu Zhang, and Ivor Tsang. Reasonable effectiveness of random weighting: A litmus test for multi-task learning. *TMLR*, 2022.
- [Liu *et al.*, 2019] Shikun Liu, Edward Johns, and Andrew J Davison. End-to-end multi-task learning with attention. In *IEEE CVPR*, pages 1871–1880, 2019.
- [Liu *et al.*, 2020] Risheng Liu, Jinyuan Liu, Zhiying Jiang, Xin Fan, and Zhongxuan Luo. A bilevel integrated model with data-driven layer ensemble for multi-modality image fusion. *IEEE TIP*, 30:1261–1274, 2020.
- [Liu *et al.*, 2021a] Jinyuan Liu, Xin Fan, Ji Jiang, Risheng Liu, and Zhongxuan Luo. Learning a deep multi-scale feature ensemble and an edge-attention guidance for image fusion. *IEEE TCSVT*, 2021.
- [Liu *et al.*, 2021b] Risheng Liu, Jiaxin Gao, Jin Zhang, Deyu Meng, and Zhouchen Lin. Investigating bi-level optimization for learning and vision from a unified perspective: A survey and beyond. *IEEE TPAMI*, 2021.
- [Liu *et al.*, 2021c] Risheng Liu, Zhu Liu, Jinyuan Liu, and Xin Fan. Searching a hierarchically aggregated fusion architecture for fast multi-modality image fusion. In *ACM MM*, pages 1600–1608, 2021.
- [Liu *et al.*, 2022a] Jinyuan Liu, Xin Fan, Zhanbo Huang, Guanyao Wu, Risheng Liu, Wei Zhong, and Zhongxuan Luo. Target-aware dual adversarial learning and a multi-scenario multi-modality benchmark to fuse infrared and visible for object detection. In *IEEE CVPR*, pages 5802–5811, 2022.
- [Liu *et al.*, 2022b] Risheng Liu, Jiaxin Gao, Xuan Liu, and Xin Fan. Revisiting gans by best-response constraint: Perspective, methodology, and application. *arXiv preprint arXiv:2205.10146*, 2022.
- [Liu *et al.*, 2023] Jinyuan Liu, Guanyao Wu, Junsheng Luan, Zhiying Jiang, Risheng Liu, and Xin Fan. Holoco: Holistic and local contrastive learning network for multi-exposure image fusion. *Information Fusion*, 95:237–249, 2023.
- [Ma *et al.*, 2017] Jinlei Ma, Zhiqiang Zhou, Bo Wang, and Hua Zong. Infrared and visible image fusion based on visual saliency map and weighted least square optimization. *Infrared Physics & Technology*, 82:8–17, 2017.
- [Ma *et al.*, 2022] Long Ma, Tengyu Ma, Risheng Liu, Xin Fan, and Zhongxuan Luo. Toward fast, flexible, and robust low-light image enhancement. *IEEE CVPR*, pages 5637–5646, 2022.
- [Sun *et al.*, 2022] Yiming Sun, Bing Cao, Pengfei Zhu, and Qinghua Hu. Detfusion: A detection-driven infrared and visible image fusion network. In *ACM MM*, pages 4003–4011, 2022.
- [Takumi *et al.*, 2017] Karasawa Takumi, Kohei Watanabe, Qishen Ha, Antonio Tejero-De-Pablos, Yoshitaka Ushiku, and Tatsuya Harada. Multispectral object detection for autonomous vehicles. In *ACM MM*, pages 35–43, 2017.
- [Tang *et al.*, 2022] Linfeng Tang, Jiteng Yuan, and Jiayi Ma. Image fusion in the loop of high-level vision tasks: A semantic-aware real-time infrared and visible image fusion network. *Information Fusion*, 82:28–42, 2022.
- [Tian *et al.*, 2019] Zhi Tian, Chunhua Shen, Hao Chen, and Tong He. Fcos: Fully convolutional one-stage object detection. In *IEEE ICCV*, pages 9627–9636, 2019.
- [Wang *et al.*, 2022] Di Wang, Jinyuan Liu, Xin Fan, and Risheng Liu. Unsupervised misaligned infrared and visible image fusion via cross-modality image generation and registration. *IJCAI*, 2022.
- [Wu *et al.*, 2022] Yuhui Wu, Zhu Liu, Jinyuan Liu, Xin Fan, and Risheng Liu. Breaking free from fusion rule: A fully semantic-driven infrared and visible image fusion. *arXiv preprint arXiv:2211.12286*, 2022.
- [Xie *et al.*, 2021] Enze Xie, Wenhui Wang, Zhiding Yu, Anima Anandkumar, Jose M Alvarez, and Ping Luo. Segformer: Simple and efficient design for semantic segmentation with transformers. *NeurIPS*, 34:12077–12090, 2021.

- [Xu *et al.*, 2019] Han Xu, Pengwei Liang, Wei Yu, Junjun Jiang, and Jiayi Ma. Learning a generative model for fusing infrared and visible images via conditional generative adversarial network with dual discriminators. In *IJCAI*, pages 3954–3960, 2019.
- [Xu *et al.*, 2022] Han Xu, Jiayi Ma, Junjun Jiang, Xiaojie Guo, and Haibin Ling. U2fusion: A unified unsupervised image fusion network. *IEEE TPAMI*, 2022.
- [Yan *et al.*, 2019] Qingsen Yan, Dong Gong, Qinfeng Shi, Anton van den Hengel, Chunhua Shen, Ian Reid, and Yanning Zhang. Attention-guided network for ghost-free high dynamic range imaging. In *IEEE CVPR*, pages 1751–1760, 2019.
- [Zhang and Ma, 2021] Hao Zhang and Jiayi Ma. Sdnet: A versatile squeeze-and-decomposition network for real-time image fusion. *IJCV*, 129(10):2761–2785, 2021.
- [Zhang *et al.*, 2021] Qiang Zhang, Shenlu Zhao, Yongjiang Luo, Dingwen Zhang, Nianchang Huang, and Jungong Han. Abmdrnet: Adaptive-weighted bi-directional modality difference reduction network for rgb-t semantic segmentation. In *IEEE CVPR*, pages 2633–2642, 2021.
- [Zhao *et al.*, 2020] Zixiang Zhao, Shuang Xu, Chunxia Zhang, Junmin Liu, Pengfei Li, and Jiangshe Zhang. Did-fuse: Deep image decomposition for infrared and visible image fusion. *IJCAI*, 2020.
- [Zhao *et al.*, 2021] Zixiang Zhao, Shuang Xu, Jiangshe Zhang, Chengyang Liang, Chunxia Zhang, and Junmin Liu. Efficient and model-based infrared and visible image fusion via algorithm unrolling. *IEEE TCSVT*, 2021.
- [Zhao *et al.*, 2022] Zixiang Zhao, Jiangshe Zhang, Shuang Xu, Zudi Lin, and Hanspeter Pfister. Discrete cosine transform network for guided depth map super-resolution. In *IEEE CVPR*, pages 5687–5697. IEEE, 2022.
- [Zhao *et al.*, 2023a] Zixiang Zhao, Haowen Bai, Jiangshe Zhang, Yulun Zhang, Shuang Xu, Zudi Lin, Radu Timofte, and Luc Van Gool. Cddfuse: Correlation-driven dual-branch feature decomposition for multi-modality image fusion. *IEEE CVPR*, 2023.
- [Zhao *et al.*, 2023b] Zixiang Zhao, Haowen Bai, Yuanzhi Zhu, Jiangshe Zhang, Shuang Xu, Yulun Zhang, Kai Zhang, Deyu Meng, Radu Timofte, and Luc Van Gool. DDFM: denoising diffusion model for multi-modality image fusion. *CoRR*, abs/2303.06840, 2023.
- [Zhou *et al.*, 2021a] Man Zhou, Jie Xiao, Yifan Chang, Xueyang Fu, Aiping Liu, Jinshan Pan, and Zheng-Jun Zha. Image de-raining via continual learning. In *IEEE CVPR*, pages 4907–4916, 2021.
- [Zhou *et al.*, 2021b] Wujie Zhou, Shaohua Dong, Caie Xu, and Yaguan Qian. Edge-aware guidance fusion network for rgb thermal scene parsing. *AAAI*, 2021.